

# Empirical relation between angular momentum transport and thermal-to-magnetic pressure ratio in shearing box simulations

E.G. Blackman<sup>1</sup> R.F. Penna<sup>1</sup>, P. Varnière<sup>1,2</sup>

1. *Dept. of Physics and Astronomy, University of Rochester, Rochester NY 14627, USA;*
2. *LAOG, Université J. Fourier UMR 5571, France*

## ABSTRACT

By combining data from different published 3-D simulations of Keplerian shearing boxes unstable to the magnetorotational instability (MRI), we highlight tight anti-correlations between the total effective inferred angular momentum transport parameter,  $\alpha_{tot}$ , its separate Maxwell and Reynolds contributions  $\alpha_{mag}$  and  $\alpha_{kin}$ , and the kinetic to magnetic pressure ratio  $\beta$ , defined with the initial or saturated (when available) thermal pressure. Plots of  $Log(\alpha_{kin})$ ,  $Log(\alpha_{mag})$ , and  $Log(\alpha_{tot})$  vs  $Log(\beta)$  are well fit by straight lines even as  $\alpha_{kin}$ ,  $\alpha_{mag}$ , and  $\alpha_{tot}$  vary by four orders of magnitude over the simulations included. The ratio  $\alpha_{kin}/\alpha_{mag}$  and the product  $\alpha_{tot}\beta$  are quite constant and largely independent of the presence or absence of weak mean fields, the choice of initial and boundary conditions, and the resolution. In short, simulations have more strongly constrained the product  $\alpha_{tot}\beta$  than  $\alpha_{tot}$  itself.

**Key Words:** accretion disks–magnetic fields–magnetohydrodynamics (MHD)–instabilities

## 1. Introduction

Accretion disks are widely appreciated to be a source of emission from gas or plasma orbiting central stars or compact objects (c.f. Frank, King, Raine 1992). In order to explain the rapid variability and short lifetimes of accreting systems without unphysical mass densities, some enhanced angular momentum transport beyond that which can be supplied by the microphysical transport coefficients is typically required. For sufficiently ionized disks, the magneto-rotational instability (MRI) offers a solution to this problem for sufficiently ionized disks (e.g. Balbus & Hawley 1991; 1998).

The MRI feeds off of an initially weak magnetic field and the turbulence induced by the ensuing instability amplifies the fluctuating magnetic energy by line stretching. Sustained magnetic fields under the influence of a shear flow in a radially decreasing angular velocity profile produce a negative magnetic (Maxwell) stress, which, in principle, produces the

dominant positive outward angular momentum transport. 3-D Simulations (e.g. Hawley, Gammie, Balbus, 1995,1996; Brandenburg et al. 1995; Stone et al. 1995) have revealed that the nonlinear evolution of systems unstable to the MRI leads to a Maxwell stress whose magnitude is larger than the negatively signed Reynolds stress. The MRI sustains the turbulent Maxwell stress and thus the outward angular momentum transport.

While the MRI has been numerically shown to provide an effective turbulent magnetic stress, incorporating the saturated state of the MRI into the framework of practical accretion disc modeling using, for example the  $\alpha_{tot}$  viscosity coefficient formalism (Shakura & Sunyaev 1973), where  $\alpha_{tot}$  is defined from the turbulent viscosity,  $\nu_T = \alpha_{tot}c_sH$  and  $c_s$  and  $H$  are the sound speed and disk scale height) suffers from the non-universality of values of  $\alpha_{tot}$  inferred from simulations. Depending on the boundary conditions, initial conditions, different treatments of viscosity and resistivity, the presence or absence of stratification, and resolution (Pessah et al. 2007), the values inferred from simulation can vary by 4 orders of magnitude (see Figs. 1 and 2 below). However, the  $\alpha_{tot}$  prescription provides a practical mean field formalism that allows a straightforward calculation of accretion disk spectra for comparison to observations by parameterizing nonlinear correlations of turbulent fluctuations by a simple closure. Developing an improved mean field theory that also incorporates the physics of the MRI, while still being practical is an important target of recent and ongoing work (e.g. Ogilvie 2003; Pessah 2006ab).

Here we emphasize that the ratio of the thermal to magnetic pressure,  $\beta$  is not generally an independent function of  $\alpha_{tot}$ , even though it is sometimes assumed to be in phenomenological analytic disc models (e.g. Yuan et al. 2005). In this paper we combine the published data extracted into Tables 1-10 to determine the empirical correlation between the kinetic and magnetic contributions to  $\alpha_{tot}$ .

In Sec. 2 we derive the formalism that relates the kinetic and magnetic parts of  $\alpha_{tot}$  to  $\beta$  for different adiabatic indices and give a physical argument for an inverse relation between  $\alpha_{tot}$  and  $\beta$ . We do not present a rigorous theory in the present work as our main focus is empirical. Toward this end, in Sec. 3 we plot the data points from published simulations and infer the empirical values for the quantities defined in Sec. 2. The data reveal that the product  $\alpha_{tot}\beta$  is nearly constant. We conclude in Sec. 4.

## 2. Maxwell and Reynolds Contributions to Transport and Relations to $\beta$

In the steady-state, ignoring microphysical viscosity, the mean azimuthal momentum equation is given by (e.g. Balbus & Hawley 1998)

$$\nabla \cdot \left[ r \rho v_\phi \mathbf{v} - r \frac{B_\phi}{4\pi} \mathbf{B}_p + r \left( P + \frac{B_p^2}{8\pi} \right) \mathbf{e}_\phi \right] = 0 \quad (1)$$

The quantity inside the brackets represents the flux of angular momentum. Of particular interest is the  $r\phi$  component of this flux, which, when greater than zero, represents the outward radial transport of angular momentum. It is given by

$$F_{r\phi} = \left[ r \rho v_\phi v_r - r \frac{B_\phi}{4\pi} B_r \right]. \quad (2)$$

Because axisymmetric accretion disk equations formally represent mean field equations, we are interested in the averaged value of  $F_{r\phi}$ . Toward obtaining this, we split the magnetic field and velocity into mean (indicated by an overbar) and fluctuating components (indicated by lower case). As in Balbus & Hawley (1998), we take the mean to represent a height integration over all  $z$ , an average over all  $\phi$  and an average over some fixed range of  $r$ . For a quantity  $Q = \overline{Q} + q$  we have  $\langle q \rangle = 0$  and

$$\langle Q \rangle = \overline{Q} = \frac{\int Q \rho d\phi dr dz}{2\pi \Sigma \Delta r}, \quad (3)$$

where  $\Sigma = \int_{-H}^H \rho dz$ . Assuming that  $\rho = \overline{\rho}$  (no fluctuating density), applying (3) to (2) gives

$$\overline{F}_{r\phi} = \frac{\Sigma r}{2H} \left[ \overline{V}_\phi \overline{V}_r - \overline{V}_{A,\phi} \overline{V}_{A,r} + \langle v_\phi v_r \rangle - \langle b_\phi b_r \rangle \right], \quad (4)$$

where  $\overline{V}_A$  is the Alfvén velocity associated with the mean field and  $\mathbf{b}$  is the Alfvén velocity associated with the fluctuating field. The first term on the right is an inward flux of angular momentum, since  $\overline{V}_r < 0$  and  $\overline{V}_\phi > 0$  at the inner most radii for an accretion disc. The remaining terms must provide the needed outward transport of angular momentum if matter is to accrete. The last two terms represent purely turbulent transport. In what follows, we assume that the mean magnetic field of smaller magnitude than the fluctuating field in saturation and that the dominant angular momentum transport comes from the last two terms of (4). (This is consistent with all of the simulations we consider.)

The shearing box simulations of Table 1 employ local Cartesian coordinates in the rotating frame. In this shearing-sheet approximation, the mean velocity  $\overline{V}_y$  vanishes at the inner most radius  $r_0$  of the shearing box, and points in the  $-\hat{y}$  for  $x = r - r_0 > 0$ , decreasing

outward in Keplerian fashion such that  $\bar{V}_y = (r - r_0)r\frac{\partial\tilde{\Omega}}{\partial r} \simeq -\frac{3}{2}\Omega x$ . Here  $\tilde{\Omega}$  is the local orbital speed,  $\Omega$  is the orbital speed of the rotating frame,  $x \equiv r - r_0$ , and  $x \ll r_0$ . In this context, we can combine the last 2 contributions of (4) into a Cartesian stress tensor

$$\bar{W}_{xy} \equiv \langle v_y v_x \rangle - \langle b_y b_x \rangle. \quad (5)$$

Using the Shakura-Sunayev prescription of  $\nu_T \equiv \alpha_{tot} c_s H$  of Sec. 1, the stress for a Keplerian flow in a shearing box that corresponds to an outward flux of angular momentum is

$$-\nu_{eff} \partial_x \bar{V}_y \simeq \frac{3}{2} \Omega \alpha_{tot} c_s H. \quad (6)$$

Setting this equal to (5) gives a closure for the stress tensor, so that

$$\alpha_{tot} = \frac{2\bar{W}_{xy}}{3\Omega c_s H} = \frac{2f(\Gamma)\bar{W}_{xy}}{3c_s^2}, \quad (7)$$

where  $\Gamma$  is the polytropic index and  $f(1) = \sqrt{\frac{1}{2}}$  (isothermal) and  $f(5/3) = \sqrt{\frac{1}{3}}$  (adiabatic). The last relation in (7) comes from solving the equation of hydrostatic equilibrium, namely

$$\frac{1}{\bar{\rho}} \frac{\partial \bar{P}}{\partial z} \simeq -\frac{GM}{R^2} \frac{z}{R}. \quad (8)$$

Over a density scale height, the solution gives  $\Omega H = \frac{c_s}{f(\Gamma)}$ , with midplane sound speed  $c_s$ .

We now split (7) into magnetic and kinetic terms such that  $\alpha_{tot} = \alpha_{kin} + \alpha_{mag}$  where

$$\alpha_{mag} \equiv -\frac{2f(\Gamma)\langle b_y b_x \rangle}{3c_s^2} = \frac{C_{mag}(\Gamma, \beta)}{\beta}, \quad (9)$$

and

$$\alpha_{kin} \equiv \frac{2f(\Gamma)\langle v_y v_x \rangle}{3c_s^2} \equiv \frac{C_{kin}(\Gamma, \beta)}{\beta}, \quad (10)$$

where  $C_{mag}(\Gamma, \beta) \equiv -\frac{4f(\Gamma)}{3\Gamma} \frac{\langle b_x b_y \rangle}{\langle b^2 \rangle}$  and  $C_{kin}(\Gamma, \beta) \equiv \frac{4f(\Gamma)}{3\Gamma} \frac{\langle v_x v_y \rangle}{\langle b^2 \rangle}$  are to be inferred from the data. We also define  $C_{tot}(\Gamma, \beta)$  such that  $\alpha_{tot} = C_{tot}/\beta$ . The statistically determined  $C_{tot}$  need not exactly equal the separately determined best fit values of  $C_{mag}$  and  $C_{kin}$ .

We can provide a crude physical argument which anticipates a strong anti-correlation between  $\alpha_{tot}$  and  $\beta$ : Note that  $\nu_{eff} = \alpha_{tot} c_s H = v_T L$ , where  $v_T$  and  $L$  are a turbulent velocity and dominant energy containing fluctuation scale. In a turbulent flow, the ratio of magnetic to kinetic turbulent energies is typically of order unity in saturation (and actually slightly larger than unity for MRI simulations). Crudely, if  $v_A \sim v_T$ , then  $\alpha_{tot} c_s H \sim v_A L$ . But  $L \sim v_T / \Omega \sim v_A / \Omega$ , if the eddy turnover time scale is comparable to the orbit time. The

latter is a reasonable assumption since the growth rate for a MRI instability that initiates turbulence is of order the rotation rate. We therefore have  $\alpha_{tot}c_sH \sim v_A^2/\Omega$  which implies  $\alpha_{tot} \sim \frac{2f(\Gamma)}{\Gamma\beta}$ , using the relations below Eq. (8). The specific anisotropy due to Keplerian shear likely implies a missing factor of order unity.

Note that  $\alpha_{mag}$ ,  $\alpha_{kin}$ ,  $\alpha_{tot}$ , and  $\beta$  were defined above as a function of the actual thermal pressure at the instant of measurement, not the initial thermal pressure of a system from which the system could evolve. For the isothermal case, the distinction is not important because the pressure is a constant in time in the simulations, but for the adiabatic case the pressure evolves. For most of the published simulations, the transport coefficients and  $\beta$  are expressed with respect to the initial pressure at the midplane  $P_0$ , where the subscript indicates both the initial time and the midplane ( $z = 0$ ). For Sano et al. (2002), data for both versions of the transport coefficients and  $\beta$  were published. Subsequently, we will explicitly distinguish the functional dependence on  $P_0$  or  $P$  where necessary. For the isothermal case we note that  $P_0 = P(0) \equiv P(z = 0)$ .

### 3. The $\alpha(\beta)$ Relation from Published Numerical Simulation Data

We have extracted data from published shearing box simulations to produce Tables 1-10. To make the numerical coefficients from the published data correspond with those of the previous section for in  $\alpha_{mag}$  and  $\alpha_{kin}$  we have multiplied the values from those references by  $\frac{2f(\Gamma)}{3\Gamma}$  in Tables 1-10. Note also that the convention used in Brandenburg 1995 (see Brandenburg 1998) is a factor of  $\frac{2}{3f(1)} \sim .48$  smaller than the convention used in the other references. Therefore, to match our numerical coefficients we have multiplied the  $\alpha$  from that reference by by  $\frac{2}{3} \frac{f(\Gamma)}{\Gamma} \frac{3}{2f(1)} = \frac{f(\Gamma)}{f(1)\Gamma}$  to construct our Table 1 for  $\alpha_{mag}$  and  $\alpha_{kin}$ . Also, the value of  $E_{mag}$  in Brandenburg et al. (1995) must be divided by a factor of 2 when placed into our definition of  $\beta$  for the magnetic pressure.

The simulations of Brandenburg et al. (1995) also differ from the others in that vertical field boundaries were used at the top and bottom of the box. This allowed mean field amplification, in contrast to the periodic boundary conditions used in the other simulations. However, since the mean field saturates at values relatively small compared to the random field, the effect of mean field growth on the total stress should be relatively small.

In Fig. 1abc we plot respectively,  $Log \alpha_{kin}(P_0)$ ,  $Log \alpha_{mag}(P_0)$ , and  $Log \alpha_{tot}(P_0)$  vs.  $Log \beta(P_0)$  for the  $\Gamma = 1$  isothermal simulations, and plot  $Log \alpha_{kin}(P_0)$  vs.  $Log \beta(P_0)$  in Fig. 1d. In Fig. 2 we show the analogous plots for the adiabatic  $\Gamma = 5/3$  cases. There the distinction between  $P$  and  $P_0$  is necessary. In Fig 2 we include the Sano et al. (2002) data

points using  $P_0$ , whereas in Fig. 3 we give the analogous plots using  $P$  rather than  $P_0$ , for the cases in which  $\alpha_{kin}(P)$ ,  $\alpha_{mag}(P)$ , and  $\beta(P)$  values are available. Although the use of  $P$  vs.  $P_0$  does not change products of the form  $\alpha\beta$ , the range of values over which the  $x$  and  $y$  axes range can differ. From Fig. 3 however, it can be seen that the best fit curves still show a tight correlation and that the  $x$  and  $y$  axes range over more than an order of magnitude supporting the same general conclusions as the previous two Figs.

The best fit solid lines are shown, with the equations for these lines at the top of each panel in Figs.1, 2, and 3. For each panel, the fit at the top is of the form  $Log(\alpha) = ALog(\beta) + D$ , shown at the top with  $A$  and  $D$  constants. We can use these fits to extract best fit values of  $C_{mag}(\Gamma, \beta)$  and  $C_{kin}(\Gamma, \beta)$  defined in Sec.2. Counter clockwise from the top right panel of Fig.1 we then have

$$C_{mag}(1) = 0.13\beta^{-0.03}, \quad (11)$$

$$C_{kin}(1) = 0.02\beta^{0.12} \quad (12)$$

$$C_{tot}(1) = 0.11\beta^{-0.06}, \quad (13)$$

and for Fig 2. we have

$$C_{mag}(5/3) = 0.10\beta(P_0)^{-0.03}, \quad (14)$$

$$C_{kin}(5/3) = 0.02\beta(P_0)^{0.01} \quad (15)$$

$$C_{tot}(5/3) = 0.08\beta(P_0)^{-0.07}, \quad (16)$$

where we have added the explicit functional dependence on  $P_0$ .

From Fig. 3 we have

$$C_{mag}(5/3) = 0.11\beta^{-0.03}, \quad (17)$$

$$C_{kin}(5/3) = 0.01\beta^{0.20} \quad (18)$$

and

$$C_{tot}(5/3) = 0.14\beta^{-0.23}. \quad (19)$$

The results for Fig 3 are based on only 8 points, yet still the weak dependence of the near constancy of  $C_{mag}$  and  $C_{tot}$  is revealed in (17) and (19). More robust are (13) and (16) which highlight a tight correlation. The results imply that  $C_{tot}(1) \sim C_{tot}(5/3)(P_0) \sim 0.1$  even as  $\alpha_{tot}(P_0)$  varies by more than 4 orders of magnitude.

The bottom right panels in Figs. 1 and 2 also highlight strict correlations between  $\alpha_{kin}$  vs.  $\alpha_{mag}$ . Fig 1d shows that the best fit for the isothermal data is  $\alpha_{kin} = 0.22\alpha_{mag}^{0.95}$  and Fig. 2d shows that for the adiabatic case,  $\alpha_{kin}(P_0) = 0.28\alpha_{mag}(P_0)$ . The near constancy of  $\alpha_{kin}/\alpha_{mag}$  was also noted by (Pessah et al. 2006ab).

#### 4. Conclusion

We have highlighted that data from published shearing box MRI simulations (Tables 1-10) show tight anti-correlations of  $\beta$  with  $\alpha_{mag}$ ,  $\alpha_{kin}$ , and their sum  $\alpha_{tot}$ . In particular, using our definitions, the product  $\alpha_{tot}\beta \sim 0.1$ , even as  $\alpha_{tot}$  varies by over 4 orders of magnitude between simulations. The data were taken from simulations invoking different codes, different vertical boundary conditions, different initial conditions, the presence or absence of stratification, the presence or absence of initial mean fields, explicit vs. numerical viscosity, different polytropic indices, and different resolutions. The data reveal that simulations have much more strongly constrained the product  $\alpha_{tot}\beta$  than any particular value of  $\alpha_{tot}$ .

The fact that no universal value of  $\alpha_{tot}$  emerges implies that the boundary and initial conditions, as well as the resolution (Pessah et al. 2007) are influencing its value. Pessah et al. (2007) show the magnitude of the magnetic stress correlates strongly with the box size. This is troubling as it implies no robust value of the transport coefficient presently emerges from simulations. In contrast, the narrow range of values for the constant product  $\alpha_{tot}\beta$  then must likely emerge from features identical in all simulations, such as the Keplerian shear profile. This is consistent with expectations from analysis of the linear regime (Pessah et al. 2006a), and more general nonlinear closures (e.g. Ogilvie 2003; Pessah et al. 2006b). More work is needed to determine the constant  $\alpha_{tot}\beta$  from first principles. Alternatively, the constants  $\alpha_{tot}\beta$  and  $\alpha_{mag}/\alpha_{kin}$  can be employed as a constraints for closures.

Modelers appealing to the MRI and extracting guidance from simulations should treat  $\alpha_{tot}$  and  $\beta$  as dependent parameters. The value of  $\alpha_{tot}\beta$  extracted from Fig. 2 emerges as much more robust universal constraint, than any specific value of  $\alpha_{tot}$ . A relation between  $\alpha_{tot}$  and  $\beta$  has been incorporated into some some disk models (e.g. Narayan et al. 1998) but not others (e.g. Yuan et al. 2005).

Note also that the data herein are for thin disks. While similar principles would apply for thick disks, the numerical constants could be different.

**Acknowledgments:** We thank A. Brandenburg, O. Gressel, A. Johansen, M. Pessah, V. Pariev, D. Uzdensky for comments and discussions. We acknowledge support from NSF grants AST-0406799, AST 00-98442, AST-0406823, NASA grant ATP04-0000-0016, the Aspen Center for Physics, and KITP of UCSB, with support from NSF Grant PHY-9907949. We acknowledge support from the Laboratory for Laser Energetics.

## REFERENCES

- Abramowicz, M., Brandenburg, A., & Lasota, J.-P. 1996, MNRAS, 281, L21
- Blackman, E. G. 1998, MNRAS, 299, L48
- Balbus S.A. & Hawley J.F., 1991, ApJ , 376 214.
- Balbus, S. A., & Hawley, J. F. 1998, Rev. Mod. Phys., 70, 1
- Brandenburg, A., Nordlund, A., Stein, R. F., & Torkelsson, U. 1995, ApJ, 446, 741
- Brandenburg, A., Nordlund, A., Stein, R. F., & Torkelsson, U. 1996, ApJ, 458, L45
- Brandenburg, A, 1998, in Theory of Black Hole Accretion Disks, ed. M. A. Abramowicz, G. Bjornsson, & J. E. Pringle (Cambridge: Cambridge Univ. Press), 61
- Hawley, J.F., Gammie C.F. & Balbus, S.A., 1995, ApJ 440, 742
- Hawley, J. F., Gammie, C. F., & Balbus, S. A. 1996, ApJ, 464, 690
- Frank J., King A., Raine D., 1992, “Accretion Power in Astrophysics,” (Cambridge: Cambridge Univ. Press).
- Narayan, R., Mahadevan, R., & Quataert, E. 1998, in Theory of Black Hole Accretion Disks, edited by Marek A. Abramowicz, Gunnlaugur Bjornsson, and James E. Pringle. Cambridge University Press, 1998., p.148
- Ogilvie, G. I. 2003, MNRAS, 340, 969
- Pessah, M. E., Chan, C.-k., & Psaltis, D. 2006, submitted to MNRAS, astro-ph/0603178
- Pessah, M. E., Chan, C.-k., & Psaltis, D. 2006, submitted to Phys. Rev. Lett.
- Pessah, M. E., Chan, C.-k., & Psaltis, D. 2007, submitted to MNRAS,
- Sano, T., & Stone, J. M. 2002, ApJ, 577, 534
- Schekochihin, A.A., Cowley, S.C., Hammett, G.W., Maron, J.L., & McWilliams, J.C. 2002, New Journal of Physics, 4, 84
- Shakura N.I. & Sunyaev R.A., 1973, A& A., 24, 337
- Stone, J. M., Hawley, J. F., Gammie, C. F., & Balbus, S. A. 1996, ApJ, 463, 656
- Yuan, F., Taam, R. E., Xue, Y., & Cui, W. 2005, ApJ in press,



Table 1. Brandenburg et al. 1995

Run	$\langle\langle 8\pi P_0/B^2 \rangle\rangle$	$(2f(\Gamma)/3\Gamma)\langle\langle -B_x B_y/4\pi P_0 \rangle\rangle$	$(2f(\Gamma)/3\Gamma)\langle\langle \rho v_x \delta v_y/P_0 \rangle\rangle$
A	154	0.000734847	0.000244949
B	143	0.000342929	9.79796E-05
C	40	0.002008582	0.000489898
D	143	0.000685857	0.000146969
E2	118	0.001126765	0.000146969
AD	40	0.001518684	0.000342929

Note. — Runs with adiabatic equations of state and vertical initial fields. All data are time- and volume-averages at late times over the turbulent layer of the disk. The magnetic field energy, Maxwell stress, and Reynolds stress are all normalized with respect to the initial gas pressure at the midplane,  $P_0$ . The run AD includes ambipolar diffusion.

Table 2. Fleming et al. 2000

Run	$\langle\langle 8\pi P_0/B^2 \rangle\rangle$	$(2f(\Gamma)/3\Gamma)\langle\langle -B_x B_y/4\pi P_0 \rangle\rangle$	$(2f(\Gamma)/3\Gamma)\langle\langle \rho v_x \delta v_y/P_0 \rangle\rangle$
BZ1	2.2222E+00	5.8659E-02	1.2009E-02
BZ2	3.6101E+00	3.9260E-02	9.2376E-03
BZ3	7.1429E+00	2.0092E-02	5.0807E-03
BZ4	1.6129E+01	9.6995E-03	2.7713E-03
ZN1	1.0000E+02	1.0392E-03	5.3116E-04
ZN2	3.3333E+02	2.3094E-04	2.3094E-04
ZN3	3.3333E+02	2.0785E-04	1.5935E-04
Y1	1.4184E+01	6.9282E-03	1.7782E-03
Y2	1.6393E+01	6.0044E-03	8.3138E-04
Y3	2.0408E+01	2.3556E-03	1.5935E-04

Note. — Runs with adiabatic equations of state. Vertical field runs are labeled by the prefix BZ, zero net  $z$  runs are labeled by the prefix ZN, and toroidal field runs are labeled by the prefix Y. All data are time- and volume-averages at late times over the turbulent layer of the disk. The magnetic field energy, Maxwell stress, and Reynolds stress are all normalized with respect to the initial gas pressure at the midplane,  $P_0$ . These runs include the effects of Ohmic resistivity.

Table 3. Hawley, Gammie, Balbus 1995

Run	$\langle\langle 8\pi P_0/B^2 \rangle\rangle$	$(2f(\Gamma)/3\Gamma)\langle\langle -B_x B_y/4\pi P_0 \rangle\rangle$	$(2f(\Gamma)/3\Gamma)\langle\langle \rho v_x \delta v_y/P_0 \rangle\rangle$
Z3	0.0294	2.678905249	0.743396207
Z4	1.9608	0.069974853	0.016165808
Z5	2.6385	0.034410076	0.013625466
Z7	2.5641	0.050575884	0.014780167
Z9	0.9346	0.121474497	0.027019993
Z12	1.0811	0.110851252	0.030022214
Z15	0.7686	0.154037052	0.032331615
Z17	3.9370	0.029329394	0.006928203
Z18	2.4038	0.061430069	0.027019993
Z19	2.1505	0.066741691	0.018475209
Z20	7.6336	0.014087347	0.003925982
Z21	6.5359	0.017089568	0.004618802
Z22	2.5974	0.049190243	0.010623245
Z23	27.0270	0.004618802	0.00092376
Z24	76.9231	0.001385641	0.00023094
Z25	30.3030	0.003233162	0.001154701
Y1	13.8889	0.007159143	0.002309401
Y2	30.3030	0.003002221	0.00092376
Y3	8.6207	0.011316065	0.003695042
Y6	23.8095	0.003002221	0.001154701
Y7	9.2593	0.008544784	0.002309401
Y8	1.6260	0.019398969	0.005080682
Y9	8.6207	0.009468544	0.002309401
Y10	62.5000	0.00069282	0.00023094
Y11	16.9492	0.005542563	0.001847521
Y12	50.0000	0.001847521	0.00069282
Y13	14.0845	0.006928203	0.002078461
Y15	8.5470	0.010854185	0.003233162
Y17	185.185	0.000508068	9.2376E-05
Y18	3.8610	0.022632131	0.006235383
YZ1	2.9674	0.019860849	0.010392305

Table 3—Continued

Run	$\langle\langle 8\pi P_0/B^2 \rangle\rangle$	$(2f(\Gamma)/3\Gamma)\langle\langle -B_x B_y/4\pi P_0 \rangle\rangle$	$(2f(\Gamma)/3\Gamma)\langle\langle \rho v_x \delta v_y/P_0 \rangle\rangle$
YZ2	3.9370	0.026789052	0.006235383

Note. — Runs with adiabatic equations of state. Vertical field runs are labeled by the prefix Z and toroidal field runs are labeled by the prefix Y. Combined toroidal and vertical field runs are labeled by the prefix YZ. All data are time- and volume-averages at late times over the turbulent layer of the disk. The magnetic field energy, Maxwell stress, and Reynolds stress are all normalized with respect to the initial gas pressure at the midplane,  $P_0$ .

Table 4. Hawley, Gammie, and Balbus 1996

Run	$\langle\langle 8\pi P_0/B^2 \rangle\rangle$	$(2f(\Gamma)/3\Gamma)\langle\langle -B_x B_y/4\pi P_0 \rangle\rangle$	$(2f(\Gamma)/3\Gamma)\langle\langle \rho v_x \delta v_y/P_0 \rangle\rangle$
R1	34	0.002817469	0.000969948
R2	63	0.001524205	0.000623538
R3	32	0.003140785	0.000969948
R4	67	0.001408735	0.00057735
R6	16	0.006189195	0.002332495
R7	250	0.000392598	0.000161658

Note. — Runs with adiabatic equations of state and random initial  $B$ . All data are time- and volume-averages at late times over the turbulent layer of the disk. The magnetic field energy, Maxwell stress, and Reynolds stress are all normalized with respect to the initial gas pressure at the midplane,  $P_0$ .

Table 5. Sano et al. 2002

Run	$\langle\langle 8\pi P_0/B^2 \rangle\rangle$	$(2f(\Gamma)/3\Gamma)\langle\langle -B_x B_y/4\pi P_0 \rangle\rangle$	$(2f(\Gamma)/3\Gamma)\langle\langle \rho v_x \delta v_y/P_0 \rangle\rangle$
Z02	2.8094E+00	3.7412E-02	7.8058E-03
Z03	4.2117E+00	2.4942E-02	5.0345E-03
Z04	1.1940E+01	9.0990E-03	2.8637E-03
S01	2.1511E+01	3.8798E-03	3.0022E-03
S03	7.7320E+00	1.2009E-02	3.0715E-03
S10	1.1988E+01	7.5286E-03	2.0346E-03
Y02	1.2686E+01	8.1522E-03	1.9237E-03
Y04	7.9931E+00	1.2494E-02	2.8868E-03

Note. — Runs with adiabatic equations of state. Vertical field runs are labeled by the prefix Z, zero net  $z$  field runs are labeled by the prefix S, and vertical field runs are labeled by the prefix Y. All data are time- and volume-averages at late times over the turbulent layer of the disk. The magnetic field energy, Maxwell stress, and Reynolds stress are all normalized with respect to the initial gas pressure at the midplane,  $P_0$ . These runs include the effects of the Hall term and Ohmic dissipation.

Table 6. Sano et al. 2002 - saturated pressure

Run	$\langle\langle P/P_0 \rangle\rangle$	$\langle\langle P \rangle\rangle/\langle\langle B^2/8\pi \rangle\rangle$	$\langle\langle w_M \rangle\rangle/\langle\langle P \rangle\rangle \cdot 2f(\Gamma)/(3\Gamma)$	$\langle\langle w_R \rangle\rangle/\langle\langle P \rangle\rangle \cdot 2f(\Gamma)/(3\Gamma)$
Z02	2.7800E+00	7.8100E+00	1.3458E-02	2.8078E-03
Z03	4.6300E+00	1.9500E+01	5.3869E-03	1.0874E-03
Z04	2.6800E+00	3.2000E+01	3.3952E-03	1.0685E-03
S01	2.5800E+00	5.5500E+01	1.5038E-03	1.1637E-03
S03	1.9400E+00	1.5000E+01	6.1901E-03	1.5832E-03
S10	3.3200E+00	3.9800E+01	2.2677E-03	6.1283E-04
Y02	6.4400E+00	8.1700E+01	1.2659E-03	2.9872E-04
Y04	5.8300E+00	4.6600E+01	2.1430E-03	4.9515E-04

Note. — Runs with adiabatic equations of state. Vertical field runs are labeled by the prefix Z, zero net  $z$  field runs are labeled by the prefix S, and vertical field runs are labeled by the prefix Y. All data are time- and volume-averages at late times over the turbulent layer of the disk. In this table,  $P$  denotes the actual pressure at the time and position of averaging. These runs include the effects of the Hall term and Ohmic dissipation.

Table 7. Stone et al. 1996

Run	$\langle\langle 8\pi P_0/B^2 \rangle\rangle$	$(2f(\Gamma)/3\Gamma)\langle\langle -B_x B_y/4\pi P_0 \rangle\rangle$	$(2f(\Gamma)/3\Gamma)\langle\langle \rho v_x \delta v_y/P_0 \rangle\rangle$
AZ1	42.2	0.001769001	0.000397217
AZ6	27.2	0.00327935	0.000739008
AY1	21.8	0.002817469	0.000672036
AL6	58.5	0.001129297	0.000274819

Note. — Runs with adiabatic equations of state. Zero net  $z$  field runs are labeled by the prefix Z. AY1 is a vertical field run and AL6 has a “flux loops” initial field configuration. All data are time- and volume-averages at late times over the turbulent layer of the disk. The magnetic field energy, Maxwell stress, and Reynolds stress are all normalized with respect to the initial gas pressure at the midplane,  $P_0$ .

Table 8. Fleming et al. 2003

Run	$\langle\langle 8\pi P(0)/B^2 \rangle\rangle$	$(2f(\Gamma)/3\Gamma)\langle\langle -B_x B_y/4\pi P(0) \rangle\rangle$	$(2f(\Gamma)/3\Gamma)\langle\langle \rho v_x \delta v_y/P(0) \rangle\rangle$
Z1	6.6667E+01	2.3570E-03	4.7140E-04
Z2	3.3333E+02	4.7140E-04	1.4142E-04
Z3	1.0000E+03	2.8284E-04	4.7140E-05
Z4	3.5714E+01	4.2426E-03	1.4142E-03
Y1	5.0000E+02	3.2998E-04	4.7140E-05
Y2	8.3333E+01	1.8856E-03	4.7140E-04

Note. — Runs with isothermal equations of state. Vertical field runs are labeled by the prefix Z and toroidal field runs are labeled by the prefix Y. All data are time- and volume-averages at late times over the turbulent layer of the disk:  $0.4 < |z/H| < 2$ . (These models also include a central “dead” zone ( $0 < |z/H| < 0.4$ ) which is not included in the averaging.) The magnetic field energy, Maxwell stress, and Reynolds stress are all normalized with respect to the midplane gas pressure,  $P(0)$ . In these models, the ionization fraction varies with height.

Table 9. Miller et al. 2000

Run	$\langle\langle 8\pi P(0)/B^2 \rangle\rangle$	$(2f(\Gamma)/3\Gamma)\langle\langle -B_x B_y/4\pi P(0) \rangle\rangle$	$(2f(\Gamma)/3\Gamma)\langle\langle \rho v_x \delta v_y/P(0) \rangle\rangle$
BY1	1.1547E+01	1.1125E-02	2.7483E-03
BY2	1.5773E+01	8.3910E-03	2.0553E-03
BY3	3.8314E+01	3.3564E-03	1.0324E-03
BY4	1.7036E+01	7.2596E-03	2.0600E-03
BY5	1.8832E+01	6.4582E-03	1.6546E-03
BY6	1.0627E+01	1.1597E-02	2.8426E-03
BYR1	1.7575E+01	6.7411E-03	1.8243E-03
BYR2	1.8018E+01	5.2326E-03	1.3435E-03
BYR3	9.1743E+00	1.6641E-02	4.0447E-03
ZN1	4.5455E+01	2.3099E-04	1.0842E-04
ZN2	2.6882E+02	2.5126E-04	1.2681E-04
BZ1	5.5804E-01	4.2756E-01	2.6823E-02
BZ2	1.1351E+00	1.4519E-01	1.6735E-02
BZ3	9.6712E-01	1.3114E-01	1.4802E-02

Note. — Runs with isothermal equations of state. Toroidal field runs are labeled by the prefix BY, zero net  $z$  field runs are labeled by the prefix ZN, and pure  $z$  field runs are labeled by the prefix BZ. “R” identifies the resistive runs. All data are time- and volume-averages at late times over the turbulent layer of the disk:  $0 < |z/H| < 2$ . (These models also include an extended, quiescent corona ( $2 < |Z/H| < 4$ ) which is not included in the averaging.) The magnetic field energy, Maxwell stress, and Reynolds stress are all normalized with respect to the midplane gas pressure,  $P(0)$ . These runs include the effects of Maxwell’s displacement current.

Table 10. Stone et al. 1996

Run	$\langle\langle 8\pi P(0)/B^2 \rangle\rangle$	$(2f(\Gamma)/3\Gamma)\langle\langle -B_x B_y/4\pi P(0) \rangle\rangle$	$(2f(\Gamma)/3\Gamma)\langle\langle \rho v_x \delta v_y/P(0) \rangle\rangle$
IZ1	6.54E+01	2.0930E-03	5.8926E-04
IZ2	2.50E+02	4.5726E-04	2.1213E-04
IZ3	6.29E+01	2.0836E-03	5.9397E-04
IZ6	4.98E+01	3.2150E-03	8.9567E-04
IY1	2.79E+01	4.6716E-03	1.1314E-03
IY2	1.63E+02	4.4312E-04	1.4991E-04
IY3	2.58E+01	3.7618E-03	9.7109E-04

Note. — Runs with isothermal equations of state. Toroidal field runs are labeled by the prefix IY and zero net  $z$  field runs are labeled by the prefix IZ. All data are time- and volume-averages over the disk at late times. The magnetic field energy, Maxwell stress, and Reynolds stress are all normalized with respect to the midplane gas pressure,  $P(0)$ .

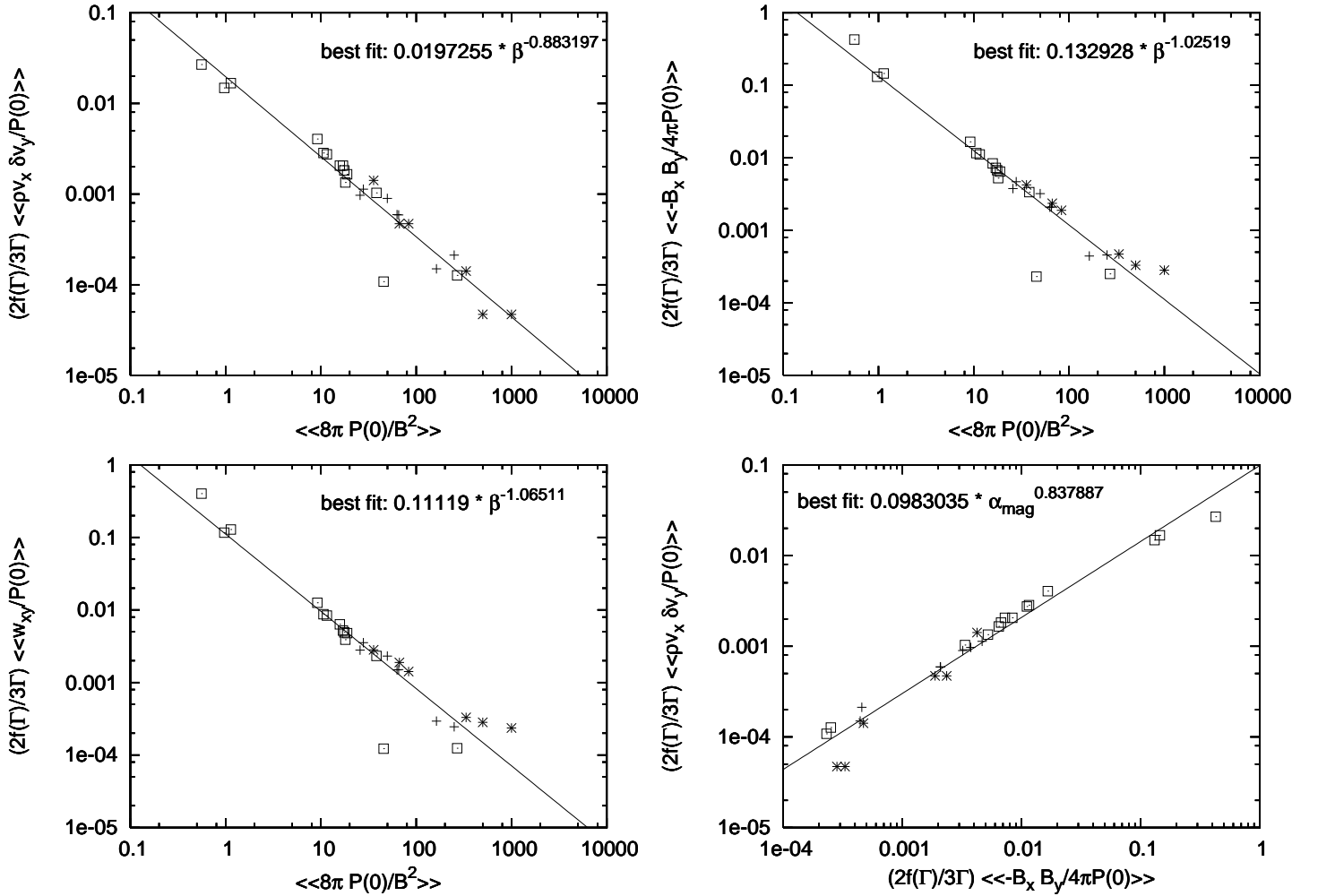


Fig. 1.— For the isothermal case, plots of  $\text{Log } \alpha_{kin}(P_0)$  and  $\text{Log } \alpha_{mag}(P_0)$  vs  $\text{Log}[\beta(P_0)]$  using the data of Tables 2-5, extracted from published simulations. In all panels, triangles are Brandenburg et al. 1995 (Table 4); Diamonds are Hawley et al. 1995 with initial  $\overline{B}_y$  (Table 3) squares are Hawley et al. 1995, with initial  $\overline{B}_z$  (Table 2); Crosses are Stone et al. 1996 (Table 5); Plusses are Hawley, Gammie, and Balbus 1996 (Table 6). Despite the different initial conditions and boundary conditions and widely ranges of  $\alpha_{mag}$ ,  $\alpha_{kin}$ , and  $\alpha_{tot}$ , the products  $\alpha\beta$  are largely constants across simulation runs. The best fits to the data are the solid lines shown, with the equations of those lines at the top of each panel with the square of correlation coefficient  $R^2$  shown

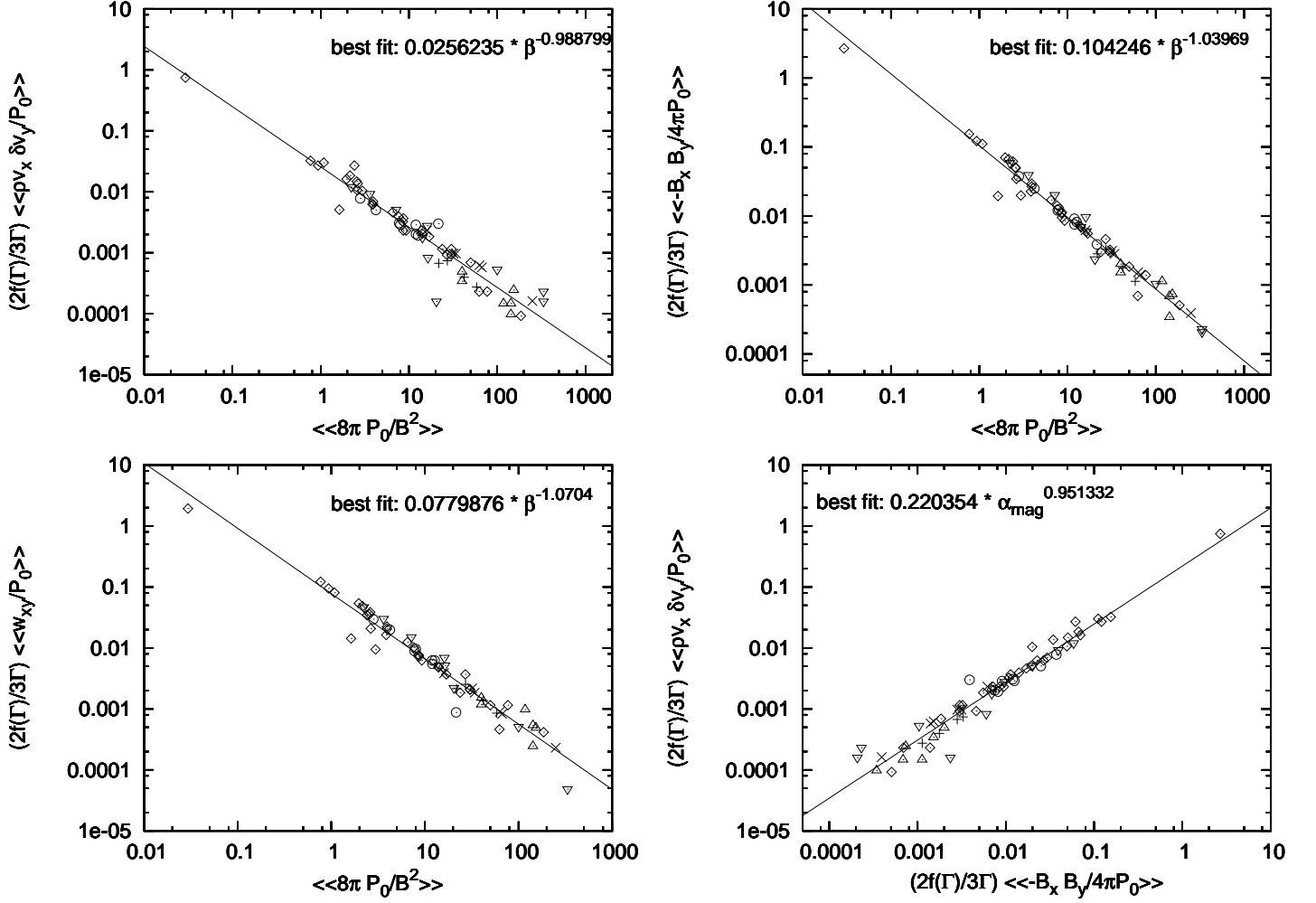


Fig. 2.— Same as Fig 1. but for the adiabatic case. Here  $P_0$  is the initial thermal pressure.

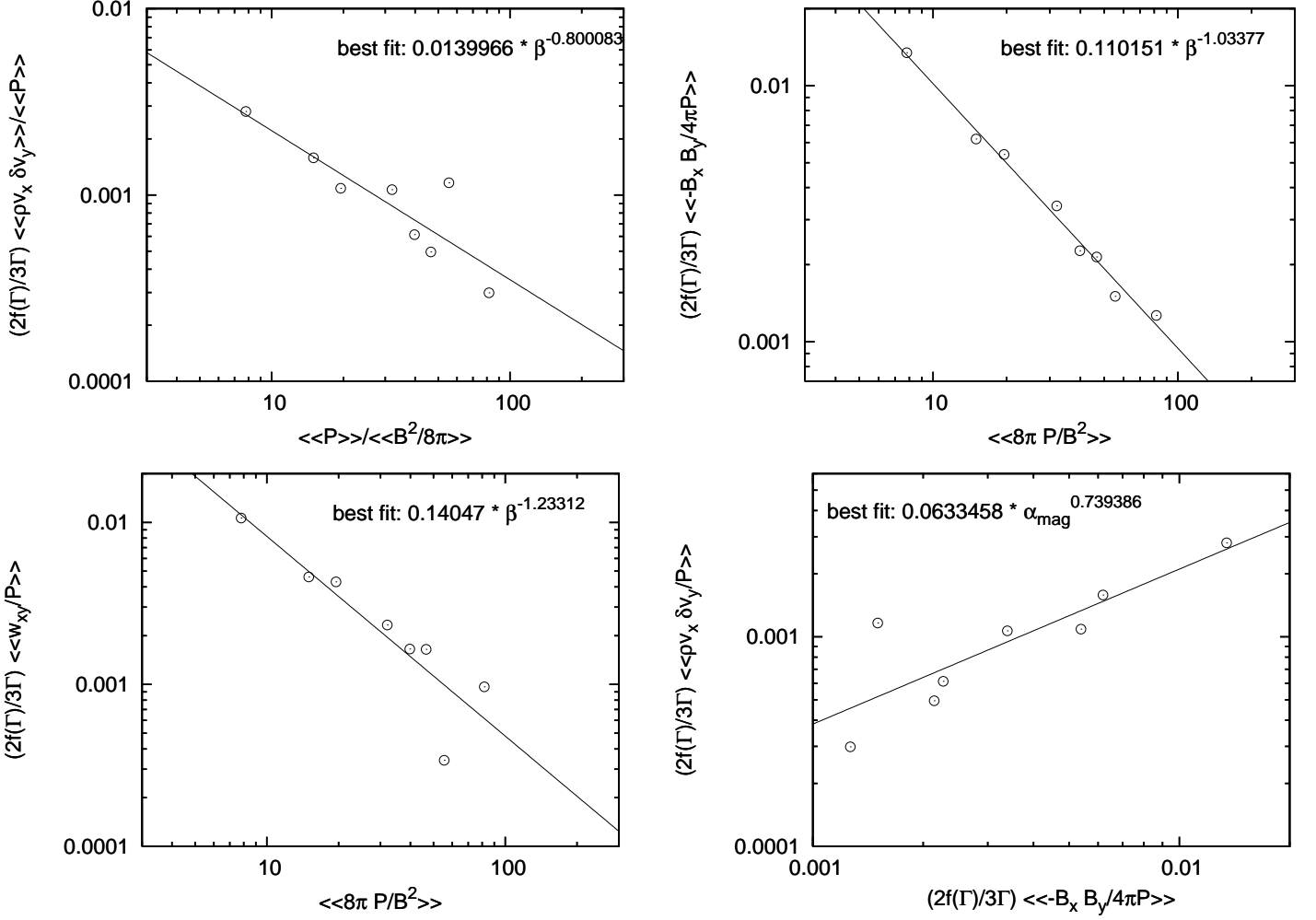


Fig. 3.— Same as Fig. 1 but using data from Sano et al. (2002) for which the saturated pressure  $P$  values are available. Here  $P$  values replace  $P_0$  used in the previous figures.